CHAPTER 3

Experimental and Analytical Method

3   EXPERIMENTAL AND ANALYTICAL METHOD

3.1   Introduction

This chapter presents the experimental and analytical procedures employed in this work. The thin film samples were deposited using a home-built radio frequency plasma enhanced chemical vapour deposition, rf PECVD system. Some samples were also thermally annealed. The as-deposited and annealed samples were put through a series of characterization procedures. These procedures were carried out on the samples according to the two categories of structure obtained for these films.

The content of this chapter is divided into two main sections. The first section introduces the rf PECVD system and presents the procedures for the sample preparation which includes the pre-deposition and film deposition procedures. Also, the substrate cleaning methods and thermal annealing processes are included. The second section presents the experimental methods employed. For each method, reviews of the corresponding analytical procedures are discussed. These analytical methods and reviews were used to discuss and assess the experimental results presented in the following chapters.

3.2   Sample Preparation

3.2.1   *Overview of radio frequency plasma enhanced chemical vapour deposition*

The home-built rf PECVD system comprised of four main components. These components include the reaction chamber, gas delivery, gas evacuation and electrical subsystems. These components are arranged according to the schematic diagram shown in Figure 3.1. The actual picture of the system can be found in Appendix 1.

The gas delivery subsystem transport gases from the gas cylinders to the deposition chamber, via a series of tubing, metering valves and controllers. The gases used were pure methane 99.995% (CH_4), nitrogen 99.995% (N_2) and hydrogen 99.995 (H_2). The flow-rates of the gases were controlled by Aalborg mass flow controllers MFCs, which operate in the ranges of 0-50 standard cubic centimetre per minute (sccm) for CH_4 and 0-200 sccm for N_2 and H_2. These gases were mixed together just before entering the chamber.

The gas evacuation subsystem comprised of a single rotary pump which acts as the "roughing" pump and a coupled water-cooled diffusion and connecting rotary pumps which were used for fine pumping. These two sets of pumps were separated by throttle valves which allow the flow direction to be selected. The set of diffusion and rotary pumps ensures a low base pressure for the chamber which helps to reduce contaminants in the chamber. To achieve good vacuum in the chamber a certain sequence in the pumping process is followed. Firstly, the chamber is pump down to approximately 3×10^{-3} mbar using the "roughing" pump. Then the flow direction was switched towards the diffusion pump (which beforehand was warmed up for

approximately 30 minutes) for "fine" pumping which enables the chamber pressure to

reach approximately 2×10^{-5} mbar. Just prior to introducing the gases into the chamber,

the flow direction was switched back to the "roughing" pump, whereby this pump also

works as the process pump. Note that the delay between the switch and the gas flow was

kept to a minimum to avoid backflow from the rotary pump towards the chamber due to
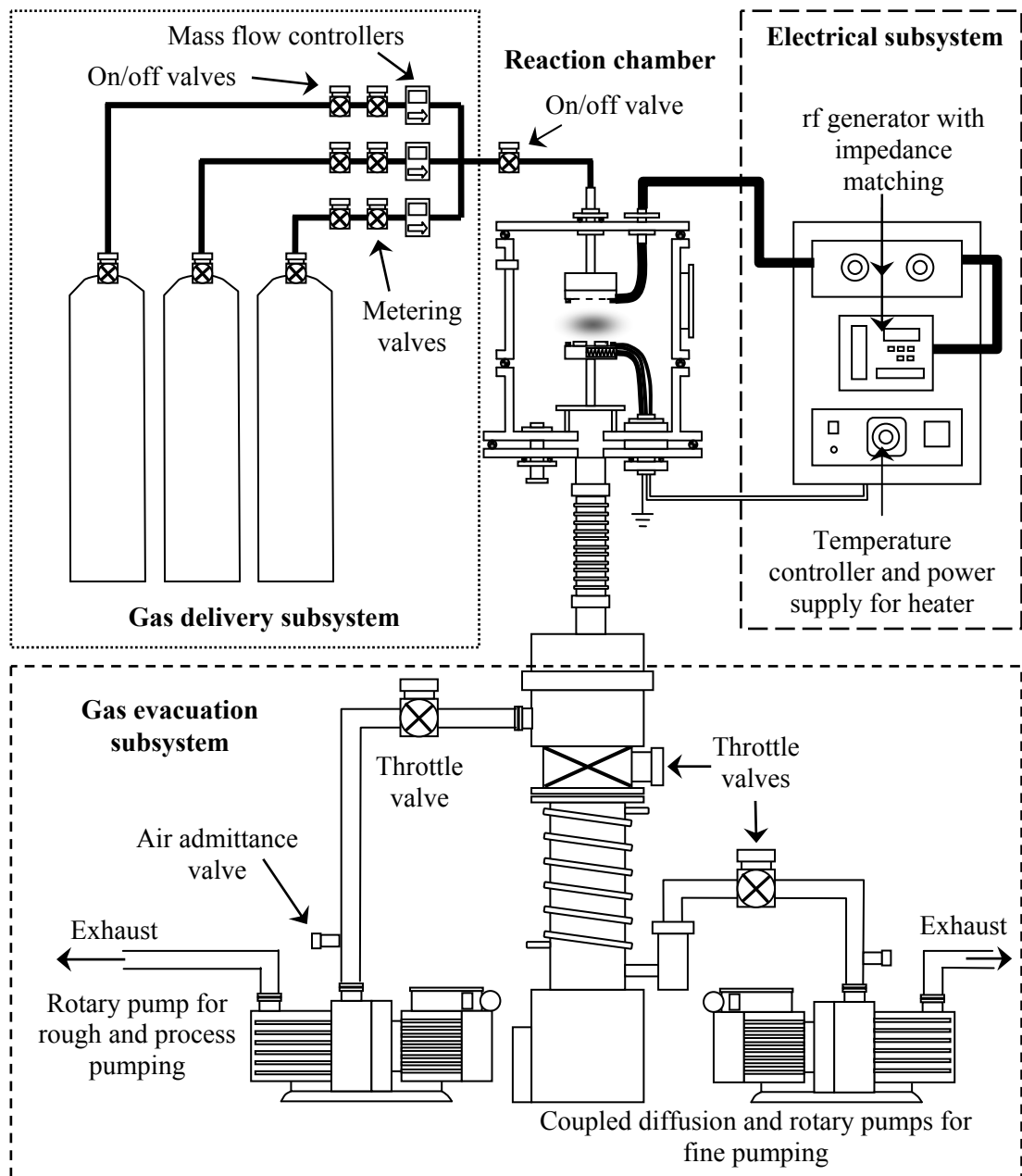
the difference in pressure.

Figure 3.1: Schematics of rf PECVD setup showing the reaction chamber and

corresponding subsystems

The electrical subsystem is comprised of a radio frequency (rf) power generator and components for substrate heating. The generator is a conventional 13.56 MHz rf power generator (model number: ENI ACG-6B). This unit is connected to a manual impedance matching network (model number: MMN 600/Pi) to compensate for the difference between the impedance of the unit and that of the system. Via this matching network the rf generator is connected to the reaction chamber. The second part of the electrical subsystem is made up of the components for the substrate heating. These include the alternating current (ac) power regulator and temperature controller (Taishio TS501). The temperature controller has an automatic switching relay which enables it to maintain the temperature of the heating element in the substrate holder by regulating the supplied ac power.

The reaction chamber proves to be the most important part of this rf PECVD system. The schematic of the chamber is shown in Figure 3.2. A parallel-plate electrode configuration is employed. The upper and bottom plates are made of 10 cm diameter stainless steel. The upper plate is connected to the rf power supply and thus acts as the powered electrode. Also, this electrode functions as the shower-head, with holes approximately 1 mm in diameter and 1 cm apart, through which the gases are flowed. A Teflon block was used as the electrical insulator for the rf powered electrode. The bottom electrode was electrically grounded and acts as the substrate holder. Here, the substrates were heated with a heating element (Watlow firerod cartridge heater, 400 W) which was positioned just underneath the substrates. The temperatures of the substrates were detected using a K-type thermocouple, arranged so that the tip touches the bottom of the substrate while still being insulated from the holder, as seen in Figure 3.2 (b). Four substrates could be mounted for each deposition and these were kept in place by an aluminium mask.
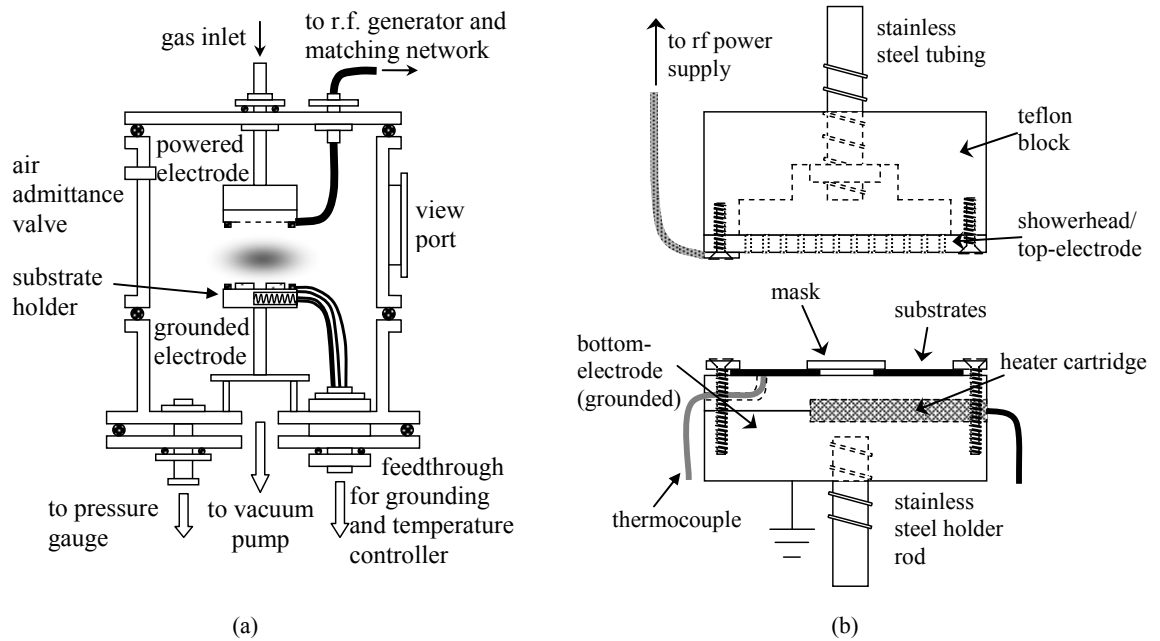
Figure 3.2: Schematic diagram and picture of home-built rf PECVD.

3.2.2   Substrate cleaning procedure

In this work, p-type (111) silicon (Si) single-crystal wafer and quartz slides were used as substrates. Two of each type of substrate were positioned on the holder for each deposition which allows extra samples to be deposited to confirm the characterization results of the films. These substrates were cut to a dimension of approximately 2.0 x 2.0 cm to match the substrate holder and mask size. The substrates were cleaned just before they are placed onto the holder, and the chamber sealed and vacuum pumped. This is to reduce the resettling of contaminants and oxidation of the cleaned surfaces, particularly for the Si substrates.

The cleaning procedures for each type of substrates are different. In the case of the quartz substrates, firstly these were immersed in a beaker of deionised water that contained a few drops of Decon90 liquid detergent. This beaker was then sonicated in

an ultra-sonic bath for 15 minutes. The quartz substrates were extracted one at a time and rinsed thoroughly with generous amount of deionised water. Finally, they were rinsed with acetone and then ethanol before being dried thoroughly in a stream of nitrogen. These process were strictly followed to ensure the removal of any contaminant especially oil deposits and also to prevent drying marks.

The cleaning procedure for Si substrates was adapted from that proposed by Kern (Kern 1993). Firstly, the substrates were boiled for 10 minutes in a hydrochloric acid solution containing a H_2O:HCl:H_2O_2 (RCA-2) ratio of 6:1:1. After this, the substrates were rinsed before being immersed in an ammonia solution with a H_2O:NH_4OH:H_2O_2 (RCA-1) ratio of 5:1:1 for two to three minutes. This is repeated for a fluoric acid solution with a H_2O:HF ratio of 10:1. Once these substrates have been thoroughly rinsed with deionised water, they were briefly dipped in ethanol and then dried in a stream of nitrogen. The RCA-2 was used to remove metal ions from the surface of the Si wafer while RCA-1 is used to remove organic residues and films. However RCA-1 tends to oxidise the Si surface leaving an undesired thin oxide layer which was subsequently removed using the HF solution.

3.2.3   Thin film deposition

To begin the deposition process, it was ensured that the reaction chamber would have been cleaned with vital components such the shower head and substrate holder polished with sand paper and clean thoroughly with acetone. Once the reaction chamber has been prepared the deposition process could begin. It was also observed that consistency and reproducibility of the deposited films greatly improved when the

position and placement of components in the setup such as the rf and grounding connections, were always kept the same. The deposition process begins with the pumping down of the chamber. With the use of the rotary and diffusion sets, the base pressure in the chamber could reach 3×10^{-5} mbar. Low base pressure minimised airborne contaminants and out-gassing in the chamber. During this process, the gas delivery line (including tubing and fittings) was opened for a moment to ensure the absence of leakage and to remove residual gases from previous deposition cycles.

Once the base pressure was achieved, the substrate was slowly heated to 100 ^{o}C which was the initial set temperature for all pre-deposition and film deposition processes. The substrate heating was done in high vacuum to minimize the chances of oxidation of the substrate surface at elevated temperatures. During this time the rf generator was warmed up for at least 15 minutes. As soon as the substrate temperature could be maintained, a pre-deposition process was carried out. Prior to introducing gases into to chamber, the vacuum pumping line was switched back to the "roughing" rotary pump which also acts as the process pump. Then immediately, H_2 is flowed into the chamber via the shower head at a fixed gas flow-rate ratio of 50 sccm. The chamber pressure was regulated at 0.8 mbar using the throttle valve. The rf power was fed to the top electrodes at a fixed value of 50 W to ignite the plasma between the powered showerhead and grounded substrate holder. The objective of this H plasma is to further remove contaminants through the effect of plasma etching and also to activate the substrate surface through the removal of bonded H atoms which results in the formation of dangling bonds. This pre-deposition process was carried out for 10 minutes. Once this is completed, the rf power supply was switched off and H_2 flow was terminated. Afterwards, the chamber was pumped back down since H_2 is not one of the precursor gas used in the film deposition.

Subsequently a mixture of CH_4 and N_2 (or CH_4 only for reference films) was introduced into the chamber for the film deposition. The flow-rates of these gases were fixed accordingly and the chamber pressure was maintained at 0.8 mbar throughout the deposition. Once the substrate temperature, flow-rates and pressure were stable, plasma was generated at a desired rf power supplied to the top (shower head) electrode. For all the film depositions, the substrate holder was grounded and the initial substrate temperature was set at 100 ^{o}C. Since the substrate holder was not intentionally cooled, its temperature increases with deposition duration for a time and then normally begins to saturate. The variation in the temperature as a function of deposition duration for different distances between the top and bottom electrodes is shown in Figure 3.3.
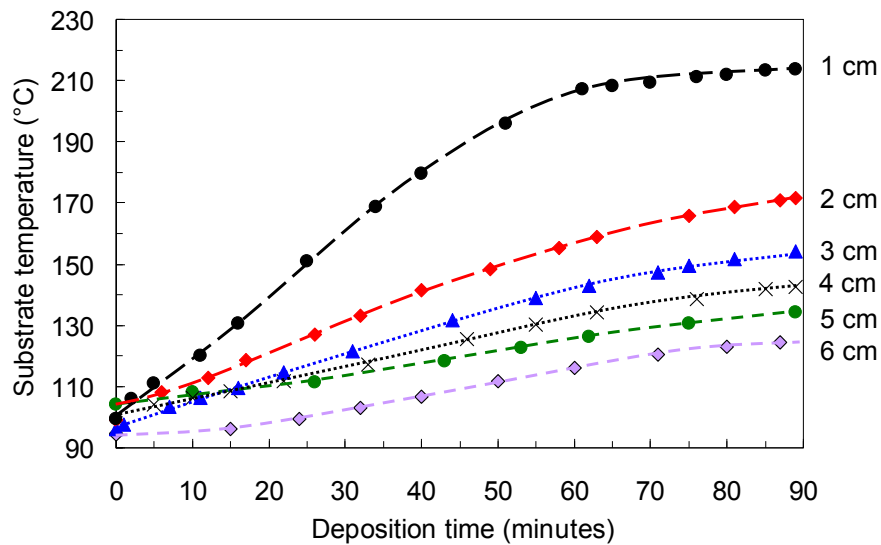

Figure 3.3: Variation in substrate temperature as a function of deposition time
at different distance between electrodes.

These changes were associated with plasma heating which increases with the decrease in the distance between these electrodes. The duration of the deposition was normally fixed at either 60 minutes for the polymeric carbon nitride films or 90 minutes

for the nanostructured films. An exception to this was the study on the effect of deposition duration whereby the duration was varied between 5 to 90 minutes.

Once the deposition process was completed, the rf power supply and the heater were switched off. During this time the throttle valves were left fully opened. Together with the gas delivery lines, the reaction chamber was pumped back down to remove all residual gases. Once the MFCs confirm the absence of gas flow, all gas valves and MFCs were closed. However the chamber was vacuum-pumped continuously until the substrate temperature decreased below 60 $^{\circ}$C. At this point the rotary pump was switched off while the throttle valves were closed to seal the chamber in vacuum. The sample was left to cool to room temperature in vacuum. This was necessary since without intentional cooling of the substrate holder, the duration needed for complete cooling would take a very long time. However once the samples were extracted out of the chamber, necessary steps were taken to characterise the samples without delay since the film may deteriorate over time. This is particularly true for the polymeric films where the sticking probability of the films to the surface is low and thus over time the films would peel off the substrates.

A summary of the deposition parameters used in this work are listed in Table 3.1. Certain parameters were kept constant for all deposition processes. These include the CH_4 gas flow-rate, initial substrate temperature and deposition pressure. For each study on the effect of a particular parameter, the parameter was varied while the others were kept constant. The varied parameters include the electrode distance, rf power, nitrogen-to-methane flow-rate ratio and deposition duration.

Table 3.1: Deposition parameters for the study of the effects of electrode distance on the structural properties of CN_x:H thin films.

	Parameter	Values
1.	Electrode distance *	6-1 cm (varied)
		or 5 cm (fixed for polymeric films)
		or 1 cm (fixed for nanostructured films)
2.	rf power *	20 – 100 W (varied)
		or 80W (fixed)
3.	Methane (CH_4) gas flow-rate	20 sccm
4.	Nitrogen (N_2) gas flow-rate *	0 – 180 sccm (varied)
		47 sccm (fixed)
5.	$[N_2/(N_2+CH_4)]$*	0 – 0.90 (varied)
		0.70 (fixed)
6.	Deposition time *	5 – 90 minutes (varied)
		90 minutes (fixed)
7.	Initial substrate temperature	100°C
8.	Chamber base pressure	$\sim 1 \times 10^{-5}$ mbar
9.	Deposition pressure	0.8 mbar

*indicates the variable parameter for each corresponding studies

3.3 Thermal Annealing

The effect of thermal annealing was carried out on a selected sample using a conventional Carbolite quartz tube furnace which functions at temperatures up to 1000 ^{o}C. The sample was annealed for 60 minutes in a nitrogen-rich ambient. Prior to the annealing processes, the furnace was calibrated to determine the region where accurate temperature set points could be achieved. This was done by recording the stable

temperature variations along the whole length of the tube using a thermocouple probe for different temperature set points and then identifying the common region of interest. Each of the selected sample to be annealed (one for each type of substrate) was cut into two parts. For the film deposited on the Si substrate, one part was cut to the size of the Fourier transform infrared (FTIR) spectrometer holder. For each annealing temperature this sample part was characterised using FTIR. Likewise, for the film deposited on the quartz substrate, one part of the sample was cut and analyzed, at each temperature increment, using Ultra Violet-visible-near infrared spectroscopy. Any changes in optical or bonding characteristics of the films at certain annealing temperatures were noted. Using these temperatures as references, the extra parts were cut into smaller pieces and these were annealed each at certain key temperatures.

To anneal the film, firstly the furnace was heated up to the required temperature. Once a stable temperature indicated by the temperature controller of the furnace has been achieved, the sample which has been placed in a ceramic boat was carefully pushed into the hot region. The film was annealed for 60 minutes. This was done for annealing temperatures in the range of $200 - 700$ ^{o}C with increments of 100 ^{o}C.

3.4   Characterization and Analytical procedures

This section describes the characterization and analytical procedures carried out to characterise the as-deposited and annealed films. Some theoretical details of the analytical methods have been described in Chapter 2. These characterization methods include a surface profilometer to determine the film thickness and growth rate, ultra violet – visible near infrared (UV-Vis-NIR) spectroscopy for optical characteristics,

photoluminescence (PL) spectroscopy for PL characteristics, Auger electron spectroscopy (AES) for elemental composition, Raman scattering spectroscopy for structural characteristics, Fourier transform infrared (FTIR) spectroscopy for chemical bonding properties, field emission scanning electron microscopy (FESEM) to obtain high resolution surface and cross-sectional images, and high resolution transmission electron microscopy (HRTEM) for atomic resolution images.

3.4.1 *Determination of growth rate measured by surface profilometry*

The growth rate of the polymeric films was calculated using the film thickness, determined from surface profilometer measurements. These measurements were carried out using a KLA-Tencor P-6 surface profiler system, shown in Figure 3.4 which works in contact mode.
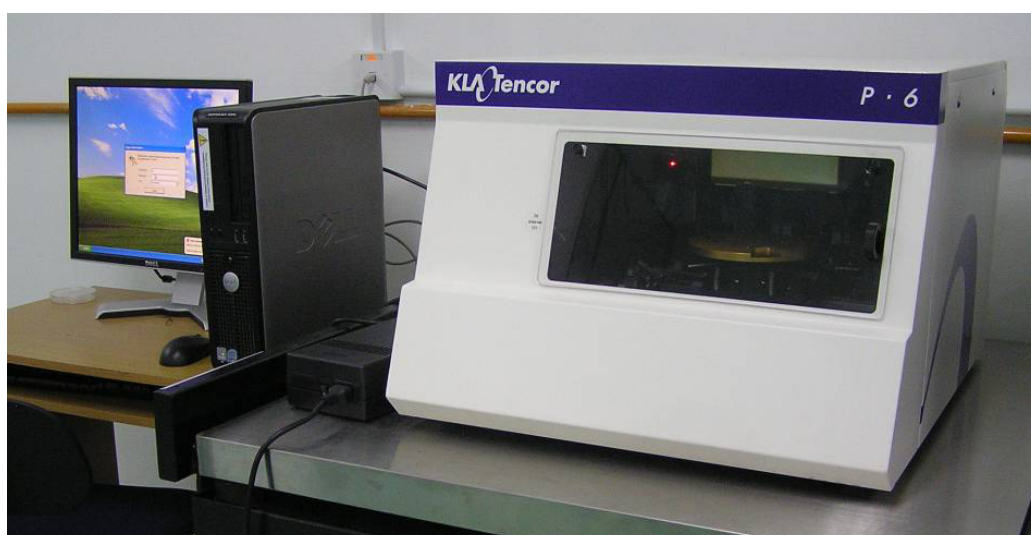

Figure 3.4: KLA-Tencor P-6 surface profilometer used for thickness measurements.

The profiler measures the step height between the edge of the film and substrate. Examples of the cross-sectional profile from these measurements are as shown in Figure 3.5. This profile depicts the different topography for films deposited as a function of rf power which is one of the studies done in the following chapters. However, it should be noted that the film thickness is not uniform and varies according to the placement of the substrates on the grounded substrate holder. This could be seen from the profile recorded for four different sides of one of the film as shown in Figure 3.6. For this reason the thickness were calculated as an average of a number of different measurements carried out on different positions on the film. Also, since the substrate placement appears to play an important role on the film growth, consistency in the placement is observed.
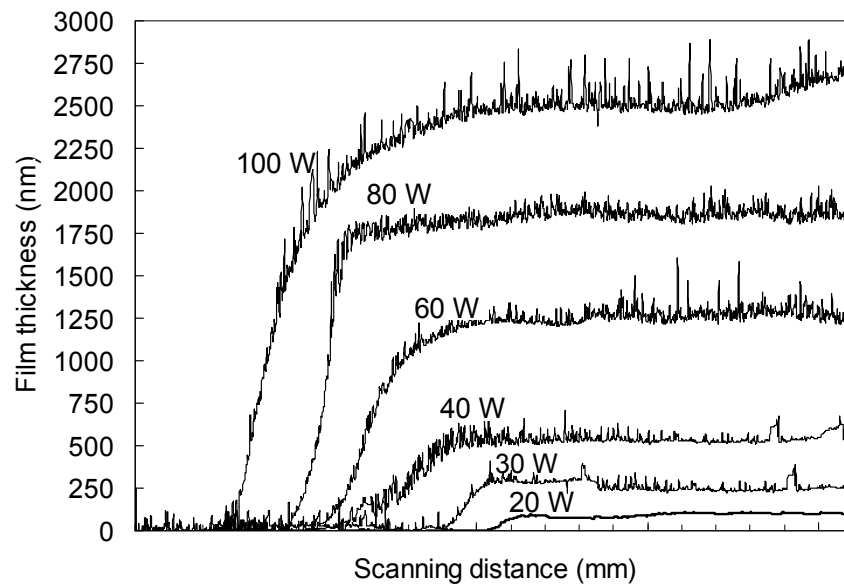

Figure 3.5: Variation of profilometer scan for varied applied rf power.

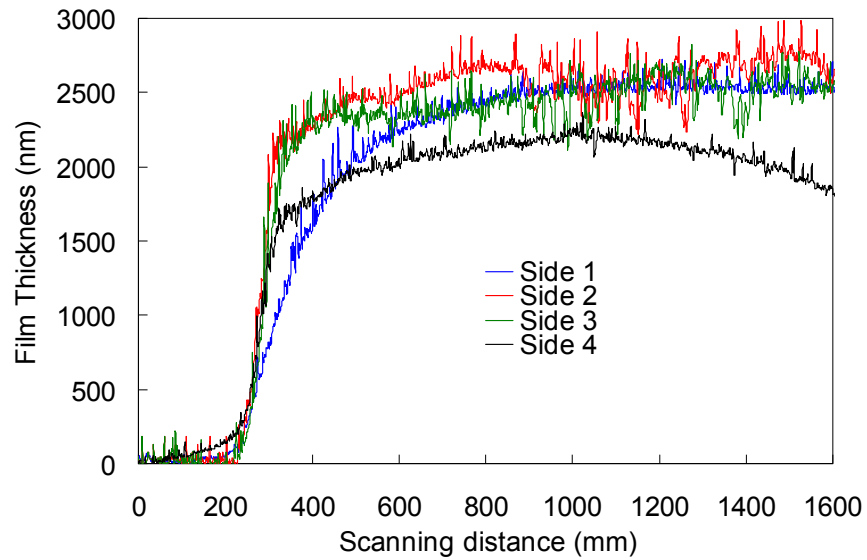Each scan is taken for thickest measured film side.

Figure 3.6: Variation of profilometer scan for film deposited at applied rf power of

100W for four different sides of the film area.

3.4.2   *Optical properties measured by ultra violet visible near infrared spectroscopy*

Optical characterization were carried out for the polymeric CN_x:H films. These were done on the films deposited on quartz using a JascoV-570 UV-Vis-NIR spectrophotometer, as shown in Figure 3.7.

Figure 3.7: JascoV-570 UV-Vis-NIR spectrophotometer used for

optical characterizations.

The measurements were carried out in both transmission and reflection modes. For the transmission measurements, the optical spectra were obtained as relative transmission with bare quartz slides used as references. Whereas, the reflectance measurements were carried out using the total reflection of an aluminium-coated glass slide as reference. The reflectance measurements were done with the incident beam angled at 5° from the normal relative to the film surface, while the transmission is measured with the beam normal to the surface.

The refractive indices of the films were calculated from the transmission spectra using the method proposed by Manifacier et al (Manifacier and et al. 1976; Phillips 1983), where the optical responses of uniform homogeneous thin films were taken into consideration. Here, the calculation based on the proposed method is described in a direct and simplified manner for clarity. According to this method, the refractive index, n of the films can be expressed as

$$n\left(\lambda_i\right)= \left[N + \left(N^2 - n_0^2\, n_1^2\right)^{\frac{1}{2}} \right]^{\frac{1}{2}} \quad\ldots\ldots\ldots\ldots\ldots\ldots(\text{Equation 3.1})$$

where
$$N = \frac{n_0^2 + n_1^2}{2} + 2\, n_0\, n_1\, \frac{T_{max} - T_{min}}{T_{max}\, T_{min}} \quad\ldots\ldots\ldots\ldots\ldots(\text{Equation 3.2})$$

n_0 is the refractive index of air taken as 1.00 and n_1 is that of quartz, the substrate used in this work and is taken as 1.50. Note that n is taken as a function of wavelength denote as $n(\lambda_i)$ since n varies with λ and $n(\lambda_i)$ is interpolated at specific λ.

T_{max} and T_{min} are the values obtained from the interference fringes of the spectrum using an envelope method as shown in Figure 3.8.
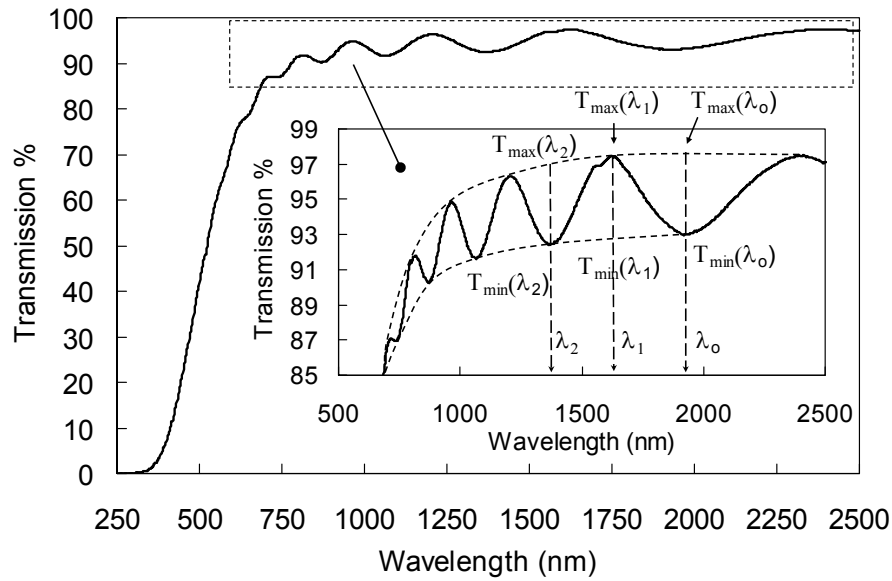
Figure 3.8: Example of optical spectrum showing the envelope method employed

on the interference fringes.

Starting at the longest wavelength, a succession of λ for each consecutive turning point whether a minima or maxima are identified and their corresponding T_{max} and T_{min} were obtained. Thus a series of λ and $n(\lambda_i)$ values were obtained. Using a combination of the method proposed by Davis et al. (Davis and et al. 1987), the variation in n as a function of λ could be simulated. This is done by utilizing Bragg's equation as shown in Equation 3.3 below.

$$m\lambda = 2nd_{opt} \ldots\ldots\ldots\ldots(\text{ Equation 3.3})$$

where d_{opt} is the optical thickness and m is the interference order. From this equation, values of nd are generated from $nd_{opt} = m\lambda/2$. Here d_{opt} is recalculated from the obtained n from Equation 3.1 and the nd_{opt} from Equation 3.3. n as a function of $1/\lambda^2$ is generated from equation 3.3.

It is generally known that nd_{opt} varies exponentially with λ, while a linear graph could be obtained from a plot of $1/\lambda^2$ versus n according to the Cauchy function (Poelman and Smet 2003):

$$n = \frac{a'}{\lambda^2} + n'_0 \ldots\ldots\ldots\ldots(\text{ Equation 3.4})$$

where a' and n'_o are the linear slope and intercept, respectively. By varying the value of m from equation (3.3) by an increment/decrement value of ½ the best fitted plot is chosen. From the generated set of data obtained from this m selection, the values of a' and n'_o are obtained. This in turn will enable the generation of n versus λ from the raw data of the UV-Vis-NIR measurement. An example is given in Figure 3.9. The final value of n for the particular sample is taken as the static refractive index which is taken at the highest wavelength where n is or is almost constant.
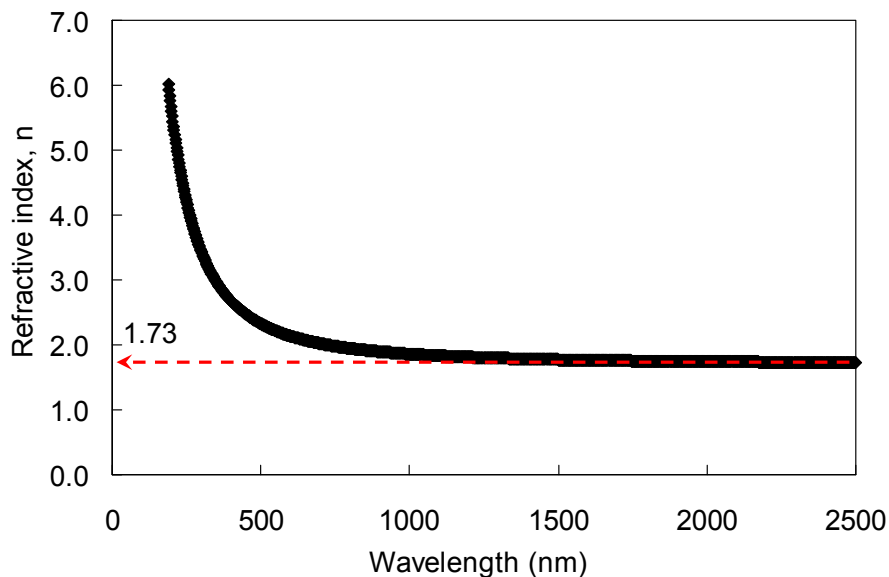

Figure 3.9: Graph showing a typical refractive index, n versus incident wavelength λ plot calculated from the raw data of UV-Vis-NIR measurement.

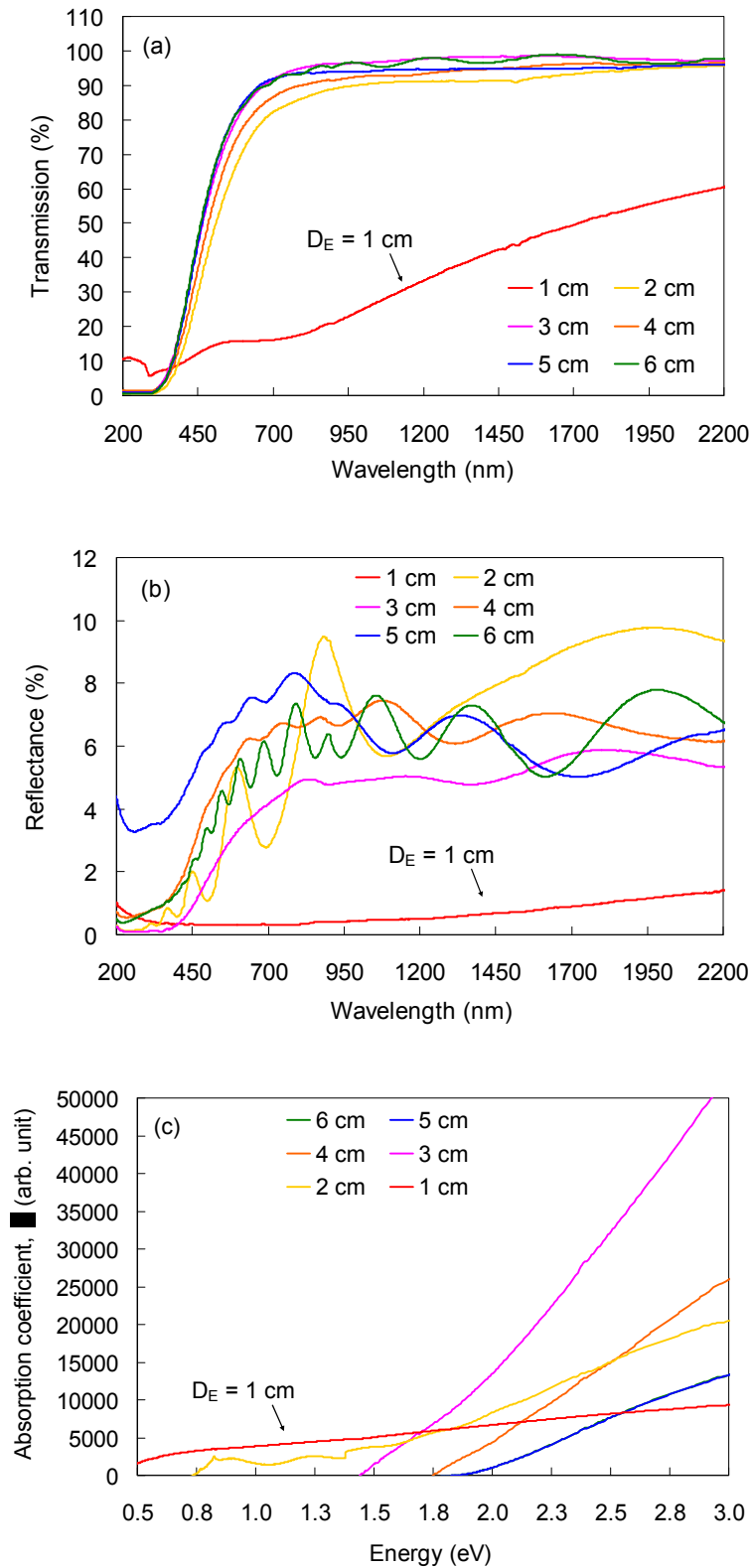Examples of the optical spectra are shown in Figure 3.10.

Figure 3.10: Variation in optical spectra in (a) transmission, (b) reflectance

and (c) calculated absorption spectra as a function of electrode distance.

The spectra shown here are those of the thin films obtained as a function of electrode distance which is used in the determination of the optical energy gap in Chapter 4. The figures include the variations in transmission, reflectance and absorption coefficient (α). α was calculated as a function of wavelength (λ) from Equation 3.5 below.

$$\alpha(\lambda) = \frac{1}{d} \ln \frac{1-T}{R} \ldots\ldots\ldots\ldots\ldots(\text{Equation 3.5})$$

where d is the film thickness, and T and R are the transmission and reflectance fractions obtained from the UV-Vis-NIR measurements. From the α graph, the values of the optical energy gap E_{04}, were interpolated. E_{04} refers to the photon energy value when the optical absorption coefficient equals 10^4 cm^{-1} (Godet et al. 2005; Zhang et al. 2000).

3.4.3   *Photoluminescence properties measured using photoluminescence spectroscopy*

Photoluminescence (PL) characteristics of the films were recorded using a Jobin Yvon HR 800 UV which is shown in Figure 3.11. A helium-cadmium laser was used with excitation wavelength of 325 nm. Appropriate filters were utilised to minimize the energy of the incident laser beam to avoid sample damage. The positions of the measured spots with dimensions of approximately one µm in diameter are carefully chosen via a magnified CCD image captured on a computer monitor. A number of measurements were carried out for each sample to verify the consistency in the measurements.
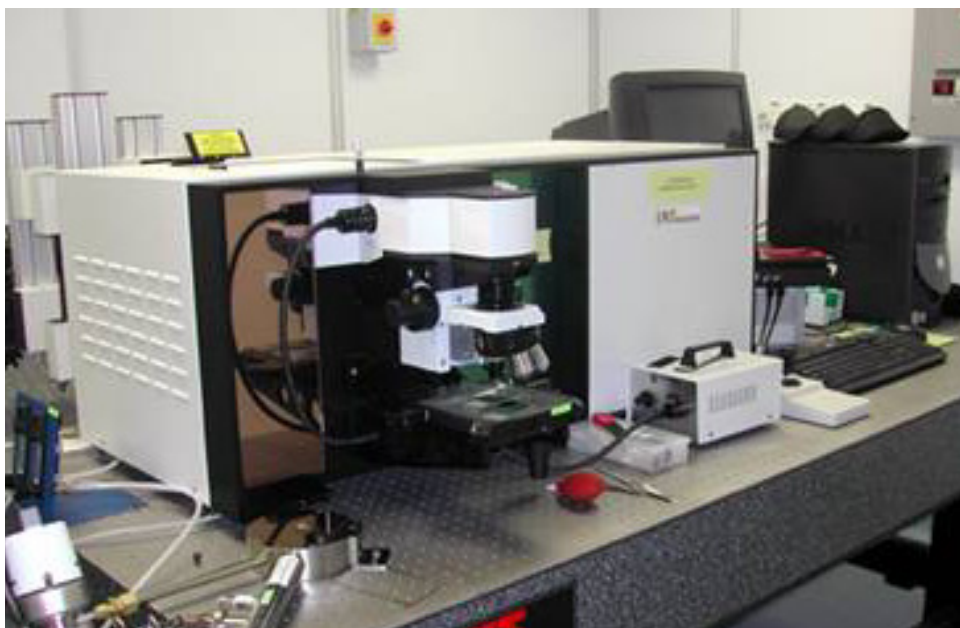
Figure 3.11: Jobin Yvon HR 800 UV Raman/photoluminescence photometer used

for photoluminescence and structural studies.

A typical PL spectrum for the polymeric carbon nitride films obtained in this work is shown in Figure 3.12. The spectrum could be deconvoluted using Gaussian fitting as shown in the example. These fittings were generated using Originlab *OriginPro* 8.1. As seen in the figure, this particular spectrum is made up of 4 overlapping bands with peaks positioned at approximately 1.93, 2.45, 3.03 and 3.24 eV. The peak positioned at 1.93 eV is not always present for all the films and from observation appears to be related to an offset correction for the baseline of the spectra. The peak at 2.45 eV is expected to be related to the presence of sp^2 clustering (Daigo and Mutsukura 2004), while the sharp, strong peak at 3.03 eV is related to the presence of nitrogen bonding in the material (Zhang et al. 1999c). The weaker peak in the range of 3.24 eV is proposed to originate from the Si substrate background (Zhang et al. 1999c).
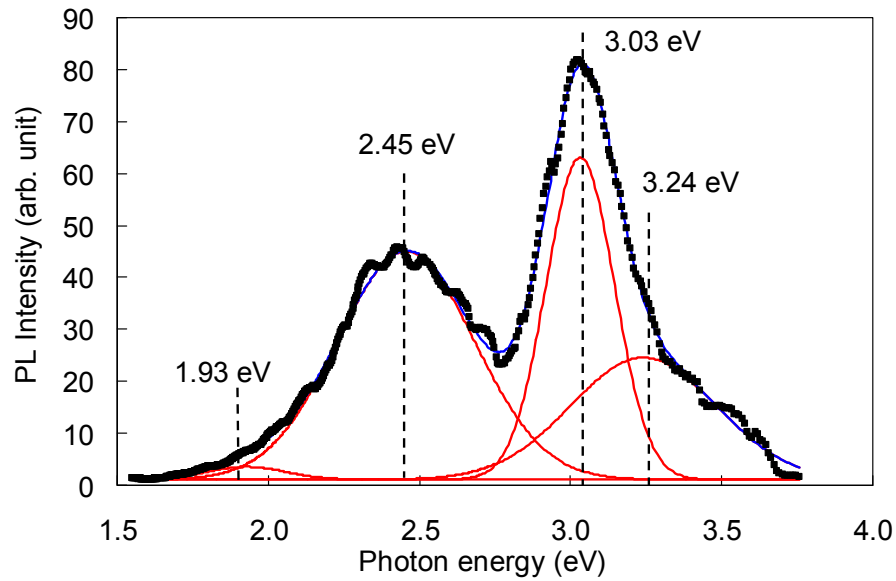
Figure 3.12: Example of photoluminescence Gaussian fitting for the film deposited at

applied rf power of 80W.

3.4.4   Elemental composition determined by Auger electron spectroscopy

Elemental composition of these CN_x:H films were studied by means of Auger

electron spectroscopy (AES) analysis. The measurements were carried out using a JEOL

JAMP-9500F field emission Auger microprobe which is shown in Figure 3.13. A series

of etch-measure cycles were carried out during AES measurement to minimize signal

distortion and variation due to potential surface contaminants. The sample was

measured at a tilt angle of 30° while the etching rate was fixed at 0.74 nms^{-1} for argon

ion beam energy of 3 keV. The example shown in Figure 3.14 below, depicts the

differences in the AES spectra of the CN_x:H films as a function of applied rf power. The

spectra clearly show the peaks assigned to C, N and oxygen O atoms in the material.

Figure 3.13: JEOL JAMP-9500F field emission Auger microprobe used for elemental
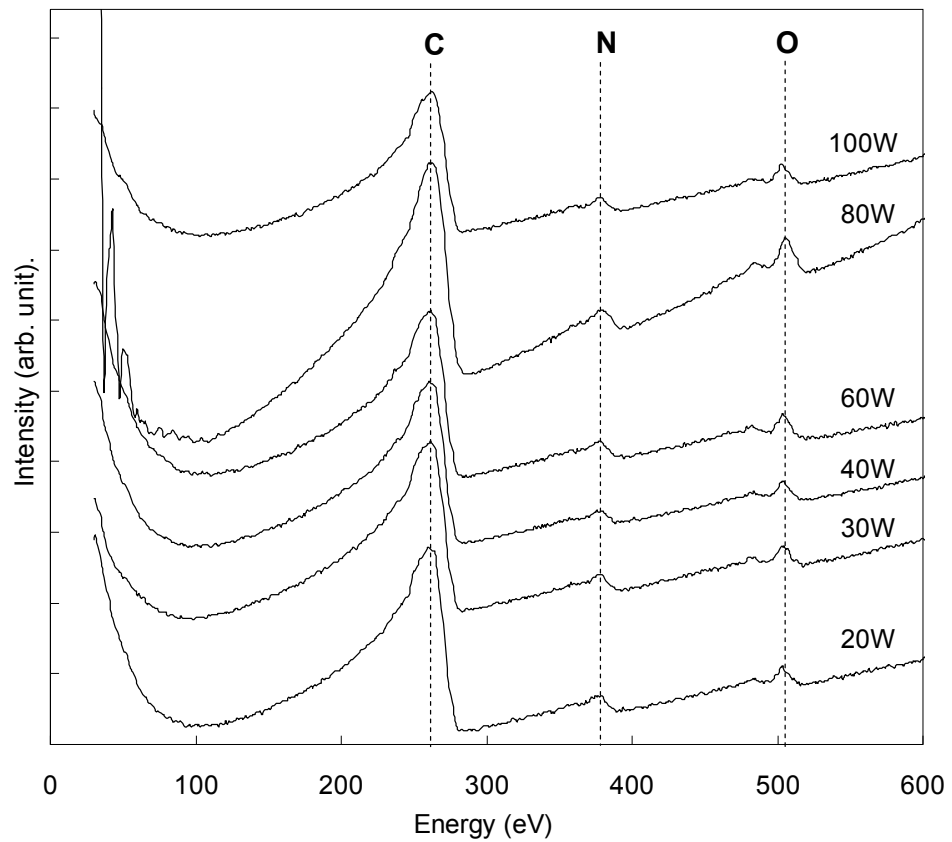
composition measurements

Figure 3.14: Example of typical Auger electron spectroscopy measurements showing

the variation in AES spectra as a function of applied rf power.

Composition quantifications were carried out using the standard sensitivity factors of the instrument. These factors are 0.250, 0.216 and 0.365 for C, N and O, respectively. The analysis and quantification of the elemental composition of the films are quite straightforward and made easy with the use of the analytical software provided with the instrument itself.

3.4.5 Structural characteristics determined by Raman scattering spectroscopy

The Raman scattering spectra of the films were recorded using a Jobin Yvon HR 800 UV. This system, being an integrated PL/Raman measuring system was also used for the PL measurements. An Ar^+ laser with excitation wavelength of 514.5 nm was used for these measurements which were carried out for films deposited on the Si substrates. The Raman shift was measured in the wavenumber range of 1000 – 2000 cm^{-1}. Examples of the raw Raman spectra are shown in Figure 3.15 (a). These spectra consist of those obtained for as-deposited films and after the film have undergone thermal annealing at 700°C.

The example spectra show the presence of D and G bands within the wavenumber range of 1360 – 1410 cm^{-1} and 1579 – 1584 cm^{-1}, respectively. To properly assess the D and G bands, the spectra is first corrected by extracting the PL background which is done by a non-linear fitting such as shown in Figure 3.15 (a). This will produce a set of corrected spectra as shown in Figure 3.15 (b). From these spectra, Gaussian fittings generated using Originlab OriginPro 8.1, were applied to deconvolute the spectra for the D and G bands. The fitting provides the peak position, FWHM and peak intensities for both the D and G bands.
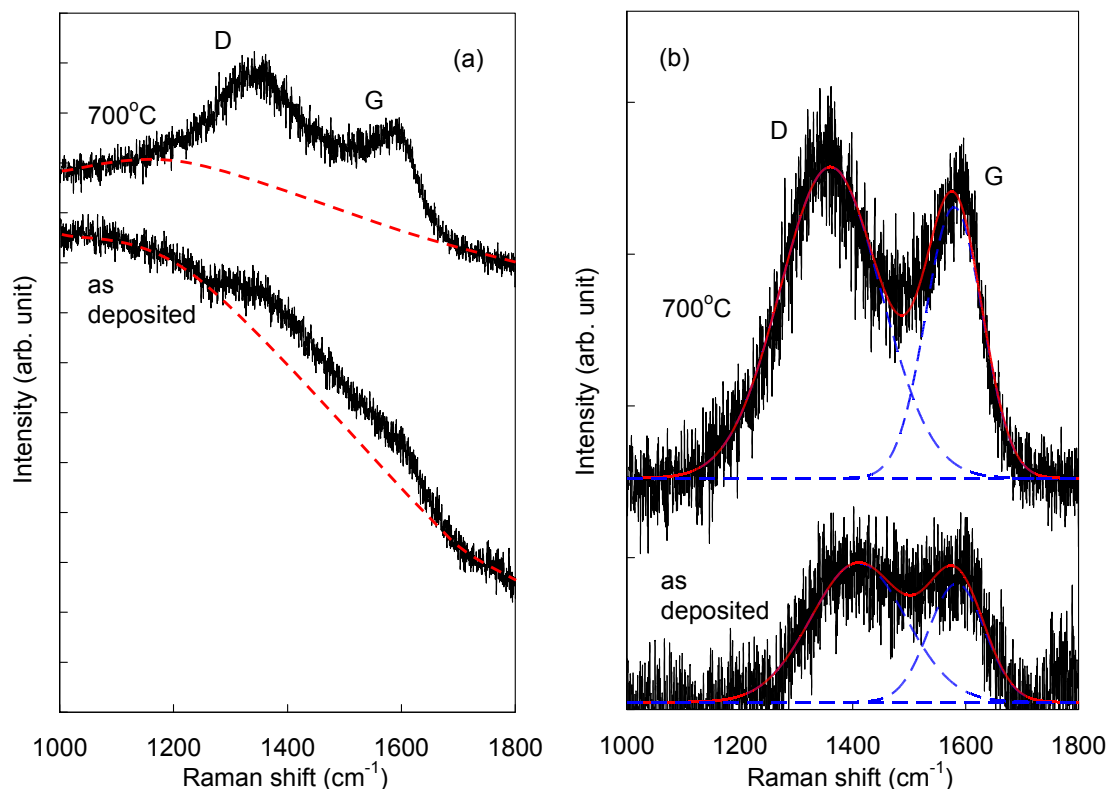
Figure 3.15: Examples of typical Raman scattering spectra with (a) raw data showing baseline fitting and (b) spectra with base line correction showing Gaussian fitting to obtain D and G bands. Examples were taken for as-deposited and thermally annealed carbon nitride films at 700 °C.

3.4.6   *Chemical bonding studies via Fourier transform infrared spectroscopy*

Chemical bonding for the carbon nitride films was studied using Fourier transform infrared (FTIR) spectroscopy. This measurement is quite common and yet a very powerful analytical tool for these films. FTIR spectra were recorded using a Perkin Elmer System 2000 FTIR which is shown in Figure 3.16. The measurements were carried out for a wavenumber range of 1000 – 4000 cm^{-1} at a resolution of 4 cm^{-1}. An average of 10 measurement cycles in transmission mode (incident beam normal to film surface) were employed to measure the films deposited on the Si substrates. A blank Si

substrate was used as reference. An example of a typical FTIR spectrum for the polymeric carbon nitride thin film is shown in Figure 3.17.

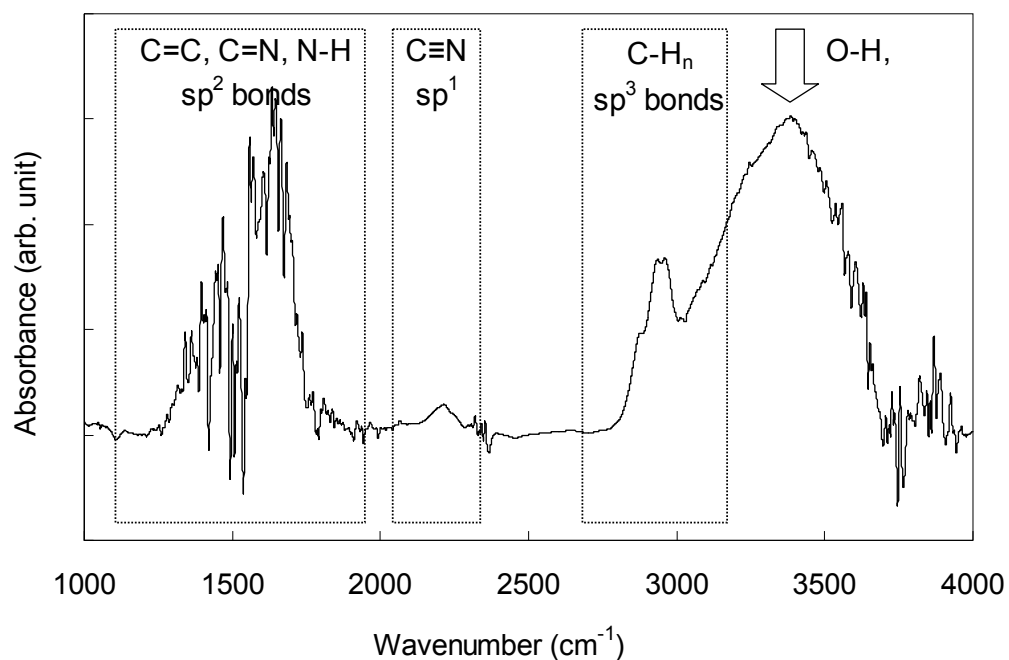Figure 3.16: Perkin Elmer System 2000 FTIR used for chemical bonding studies.

Figure 3.17: Example of typical Fourier transform infrared spectrum

for carbon nitride films

As in this example, the FTIR spectra in the following chapters are shown as the stacking of the absorbance of the film normalized to the film thickness. Apart from the plot of the whole 1000 – 4000 cm^{-1} range, individual plots within the range of 1300 – 1900 cm^{-1}, 1800 – 2400 cm^{-1} and 2600 – 3800 cm^{-1} as shown in Figure 3.18, are plotted for clarification. Using the peak assignments presented in Chapter 2 Table 2.1 the spectra within the selected ranges were deconvoluted using Gaussian fitting. The corresponding examples are shown in Figure 3.19. From these fittings the assessment of different bonds and functional groups which includes the D/G ratio, sp^2/sp^3 ratio and the variation in C≡N and C=N were done. For the polymeric films in this work, the fittings were carried out fully. A full list of the variations is compiled as an attachment in Appendix 2. However, for the nanostructured films, the differences in the structure and morphology seen with the changes in deposition parameters suggest that the correction of the spectra against their film thicknesses may not yield accurate spectral normalization. Thus, in depth assessment in regards to relative intensities were avoided for these nanostructured films.
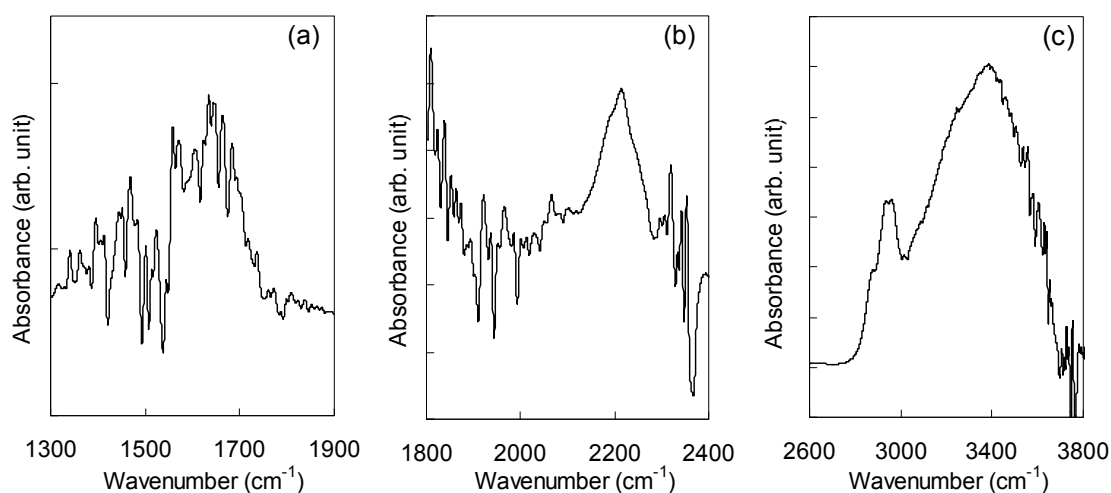

Figure 3.18: Example of typical separation of Fourier transform infrared spectrum into three different spectra range of (a) 1300-1900 cm^{-1}, (b) 1800-2400 cm^{-1} and (c) 2600-3800 cm^{-1}.
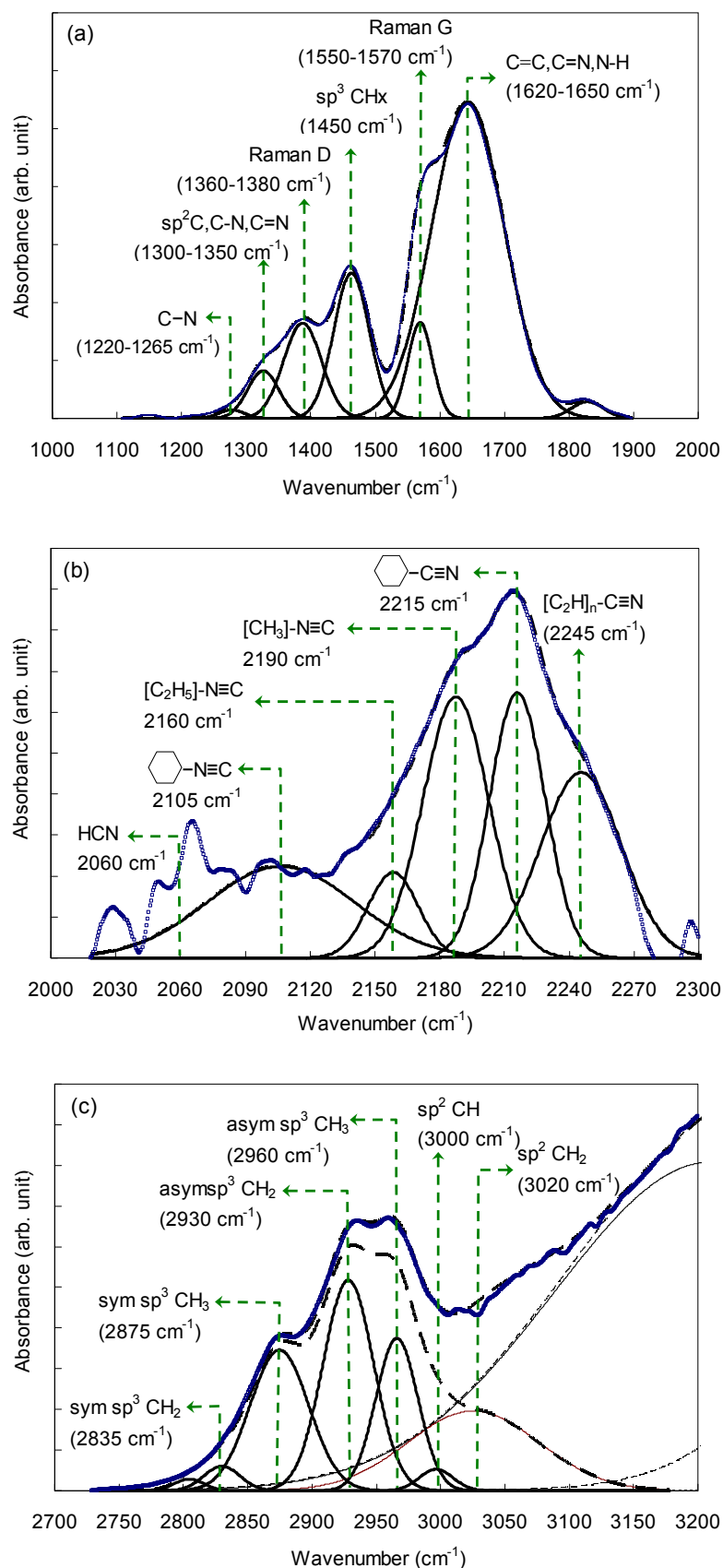
Figure 3.19: Example of the deconvolution of FTIR spectra using Gaussian fitting for

the spectra range of (a) 1000-2000 cm^{-1}, (b) 2000-2300 cm^{-1} and (c) 2700-3200 cm^{-1}.

Also shown are the peak positions for the functional groups of interest.

As seen in Figure 3.19 (a) the D/G ratio is also available from the absorbance intensity in the wavelength range of 1000-1900 cm^{-1} of the FTIR spectrum. However it was found as the study progressed that there appears to be no correlation between the D and G peaks of the FTIR and Raman measurements. This is similar to the argument by Ferrari et al. (Ferrari and Robertson 2000; Ferrari et al. 2003b) and for this the assessment of D/G ratio from FTIR was avoided. The sp^2/sp^3 ratios were calculated from the ratio of the sum of the integrated intensities of the sp^2 and sp^3 –C peaks obtained from the wavelength region of 2700-3200 cm^{-1}. Prior to that baseline corrections was carried out by fitting and extracting the O-H and/or N-H peaks from the spectra. On the other hand, the variation in the double bonds sp^2–C correlated with the C=C, C=N and/or N–H bonds was calculated from the single sharp, strong peak at approximately 1620-1650 cm^{-1}. The sp^1 isonitrile and nitrile bonds were obtained from the region of 2000-2300 cm^{-1}. These were analyzed as individual peaks corresponding to their own functional groups.

3.4.7   High resolution surface and cross-sectional images obtained using field emission scanning electron microscopy

Surface and cross-sectional images were taken to study the morphology of the nanostructured carbon nitride films. These high resolution images were taken using a FEI Quanta 200 field emission scanning electron microscope (FESEM), which is shown in Figure 3.20. The images were taken at high vacuum at an acceleration voltage of 20 kV. Once the sample surface was roughly scanned, three different increasing magnifications were used to obtain the images on a selected spot. The position of this spot was usually taken close to the edge of the sample where the sample would have

been cleaved for cross-sectional image scanning. To obtain the cross-sectional image, the sample was mounted "edge up" which was made easy since the FESEM sample holder is made in such a way as to allow vertical positioning of the mounting stub. This sample could be positioned almost vertically and thus negates the tilting requirement for such images to be taken. Prior to the FESEM scan of the samples, a "splash" of Au was-deposited onto the films. This was done using a sputter coated with an Au foil as target. The purpose of this is to reduce surface charging effect to improve the image resolution.

Figure 3.20: FEI Quanta 200 field emission scanning electron (FESEM) microscope used for surface and cross-sectional high-resolution imaging of carbon nitride films.

3.4.8   *Atomic-resolution images obtained using high-resolution transmission electron microscopy*

High-resolution transmission electron microscope (HRTEM) micrographs were obtained using a JEOL JEM-2100F (Figure 3.21) operating at 200 kV acceleration voltage. These atomic resolution images are used to identify the structural order for the

nanostructured carbon nitride films. However due to the limited accessibility and high charging fee for the use of this equipment, only one sample could be evaluated. The sample was chosen by referring particularly to its FESEM images. The HRTEM used was also equipped with an energy dispersive x-ray (EDX) and selected area electron diffraction (SAED) analyzers. Using these analyzers the SAED pattern and high-resolution EDX analysis on different part of an individual strand on the nanostructure were analyzed.

To prepare the samples for the HRTEM analysis, firstly the samples were scratched off the substrate using a spatula. The sample was dispersed onto a small amount of acetone which was then scooped out using a copper grid. Due to the nature of the sample preparation the samples attained on these grids may bunch up together which makes them unsuitable for the imaging. Thus, efforts were made to find scattered strands which were well dispersed and allow proper imaging and analysis.

Figure 3.21: JEOL JEM-2100F high resolution transmission electron microscope used for high resolution imaging of individual nanostructured carbon nitride strands, energy dispersive x-ray (EDX) and selected area electron diffraction (SAED) analysis.